6ICEGE 6th International Conference on Earthquake Geotechnical Engineering
1-4 November 2015
Christchurch, New Zealand

Seismic Isolation Effects and Elastic Response Spectra of Liquefied Ground

G.D. Bouckovalas[1], Y.Z. Tsiapas[2]

ABSTRACT

Liquefiable sites may amplify or de-amplify the seismic ground motion, depending on two main factors: the onset of liquefaction relative (before or after) to the strong motion part of the seismic excitation and the capacity of the layer to attenuate the seismic excitation when it liquefies. These mechanisms are explored herein with the aid of three liquefaction case histories and a number of advanced numerical analyses. Conclusions are drawn on the capacity of liquefiable soil layers to filter out a range of harmonic excitation components, and thus provide a kind of "natural seismic isolation" for the superstructure, while two alternative methods are proposed for a simplified (e.g. SHAKE-type) computation of free field elastic response spectra for liquefiable sites.

Introduction

Among the various design issues related with earthquake-induced liquefaction, the free field response is probably the least considered by the research community today. One possible reason is that the current practice is overwhelming in favor of pile foundations, which transfer the structure loads to deeper non-liquefiable strata, combined with soil improvement over the entire liquefaction depth aimed to minimize the lateral loads applied upon the piles. However, this practice has started to be challenged in recent years (e.g. Cascone & Bouckovalas 1998; Dashti et al. 2010; Dimitriadi 2014; Karamitros et al. 2012 & 2013; Liu & Dobry 1997; Naesgaard et al. 1998) as there is evidence that the existence of a shear resistant non-liquefiable crust (e.g. natural clay or stone column densified sand) on top of the liquefiable soil layers may moderate the detrimental liquefaction effects and satisfy performance criteria for shallow foundations. The additional benefit from such an innovative design would be to reduce inertia loads on the superstructure as the liquefiable layers below the crust may act as a form of “natural seismic isolation”. In view of these new developments, the free field liquefied ground response attracts renewed interest as it constitutes basic input for the seismic design of the structure and the foundation.

Within the above research framework, the first issue addressed in this paper refers to the capacity of liquefied soil layers to attenuate the seismic motion, i.e. to provide natural seismic isolation. To become more specific, driven by a number of early observations and well documented case studies (e.g. Kawasumi 1968; Iwasaki & Tai 1996), it has become common notion that earthquake-induced soil liquefaction will diminish the free field seismic ground motion. However, there is also recent evidence about the opposite (e.g. Dashti et al. 2010; Youd & Carter

[1]Professor, Geotechnical Department, N.T.U.A, Athens, Greece, gbouck@central.ntua.gr
[2]Ph.D. Candidate, Geotechnical Department, N.T.U.A, Athens, Greece, ioannis.tsiapas@gmail.com

2005), i.e. that liquefaction in the subsoil may have a minor effect or even lead to amplification of the seismic ground motion. Such evidence usually comes from cases when liquefaction occurred after the strong motion part of the seismic excitation or in the presence of relatively thin liquefiable soil layers. These seemingly contradictory trends are explored herein, with the aid of parametric numerical analyses aimed to identify and establish quantitative criteria for the soil and excitation conditions which control the seismic response of liquefied sites.

The second issue which is addressed in the paper is related to the prediction of the free field elastic response spectra for liquefiable sites. There is no question that such predictions can be obtained today using available non-linear (Finite Difference or Finite Element) numerical algorithms. However, such analyses are still out of bounds for the majority of engineers, who seek much simpler means in order to solve liquefaction related applications, such as SHAKE-type equivalent linear analyses. Along this line, two new analytical methodologies have been developed, which allow a simplified prediction of the elastic response spectra of liquefied ground while taking consistently into account the pre- as well as the post-liquefaction segments of the seismic excitation. In the first one ("interpolation methodology"), it is assumed that the response spectra for non-liquefied and for totally liquefied ground constitute upper and lower bounds to the actual spectrum. In the second one ("superposition methodology"), the actual spectrum is regarded as the envelope of the response spectra computed separately for the pre- and the post-liquefaction segments of the seismic motion. The proposed methodologies are calibrated against the seismic motion recordings from 3 liquefaction case histories, and the results of parametric, numerical analyses with FLAC combined with the NTUA-Sand constitutive model.

Seismic Isolation Capacity of Liquefied Soil Layers

Parametric Numerical Analyses

The effect of the liquefied layer thickness on the amplification (or the de-amplification) of ground motion, as well as the existence of simple criteria for the estimation of the minimum thickness required for a liquefied soil layer to act as natural isolation were explored with the aid parametric numerical analyses of the free field response. The analyses were performed with the finite difference code FLAC (Itasca 2011), in a fully coupled, non-linear, dynamic form. The examined soil profile (Figure 1) consists of a non-liquefiable clay crust, underlain by a liquefiable sand layer of variable thickness and a non-liquefiable clay bed. The NTUA-Sand critical state plasticity constitutive model (Andrianopoulos et al. 2010; Karamitros 2010) was employed to simulate the liquefiable sand response, while a simpler Ramberg & Osgood type hysteretic constitutive model was selected for the non-liquefiable top and bed clay layers. The NTUA-Sand model was calibrated against static and cyclic tests on saturated fine Nevada Sand (Arulmoli et al. 1992) while the Ramberg & Osgood (1943) model was calibrated against the experimental modulus reduction and damping curves of Vucetic & Dobry (1991).

A total of about 290 parametric analyses were performed with the finite difference mesh shown in Figure 1, consisting of a single element column with 14m depth and element zone size 1m x 0.50m (width x height). Tied–node conditions are considered at the lateral boundaries, which impose the same displacements to grid points of the same elevation. The base of the soil column was shaken with a 15-cycle harmonic excitation, with maximum acceleration a_{max} = 0.1 – 0.4g

and frequency f = 2 – 10 Hz. The plasticity index of the clay layers is PI = 30%, whereas the shear wave velocity equals V_S = 100 and 300 m/sec, for the clay crust and the clay bed layers respectively. The relative density of the sand varied in the range D_r = 40 – 75%, while the associated permeability coefficient has been increased from k = 0 to 0.06 cm/sec. The thickness of the clay crust and the liquefied sand layers varied in the range H_{crust} = 2 – 6m and H_{liq} = 1 – 12m respectively (at 1m increments), while the thickness of the clay bed was properly adjusted so that the total height of the column remained equal to 14m.

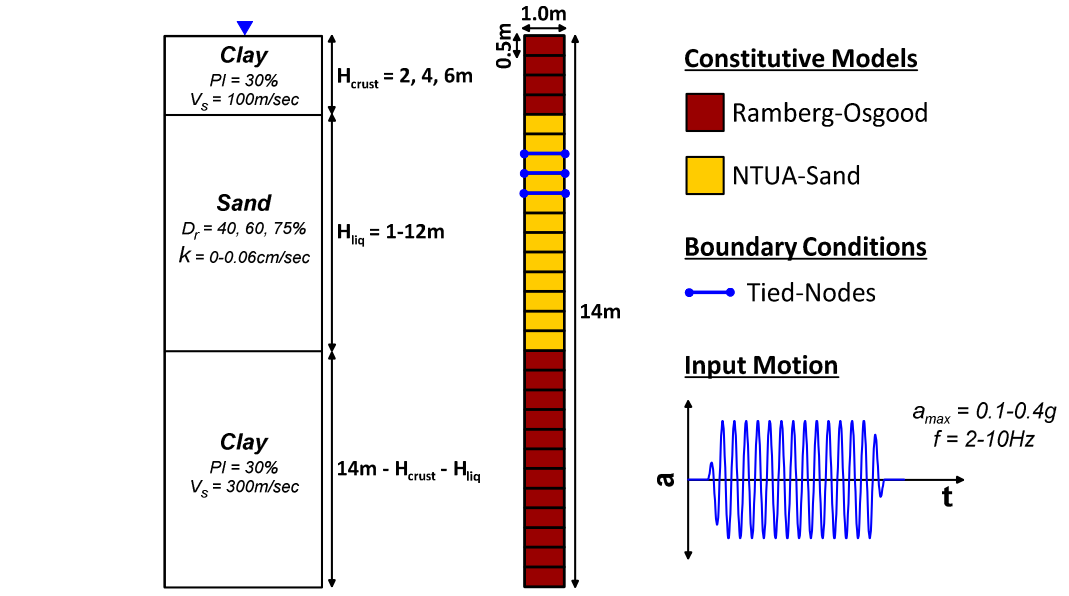

Figure 1. Soil profile and finite difference mesh.

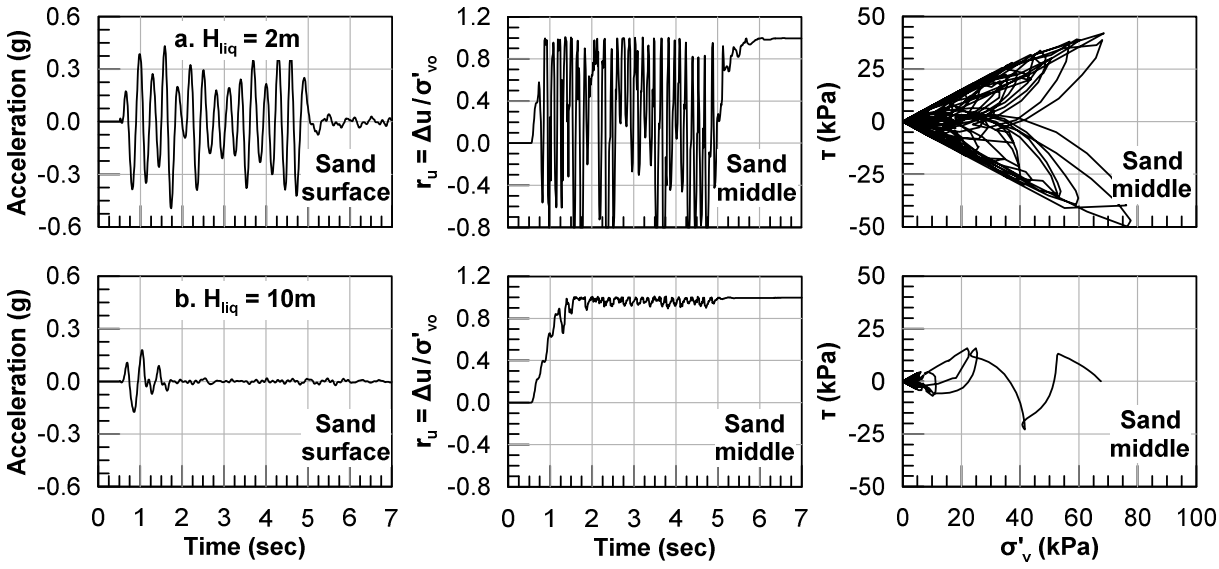

Figure 2. Typical acceleration and excess pore pressure ratio time-histories, as well as stress paths for different values of H_{liq}.

Figure 2 shows typical numerical predictions of special interest for the present study, namely the acceleration time-histories at the sand surface, the time-history of excess pore pressure ratio $r_u=\Delta u/\sigma'_{v,o}$ at mid-depth of the sand layer, as well as, the associated stress paths $\tau - \sigma'_v$ (Δu denotes the excess pore pressure, τ and σ'_v the applied shear and vertical effective stresses respectively, while the "o" index indicates initial geostatic conditions). The predictions refer to the baseline input parameters (i.e. a_{max} = 0.3g, f = 3.3Hz, H_{crust} = 2m, D_r = 60%, k = 0) and two distinctly different liquefiable sand layers: a "thin" (H_{liq} = 2m) and a "thick" (H_{liq} = 10m)one. It is worth to observe that the conventionally expected seismic isolation effect is only exhibited by the "thick" sand layer (Figure 2b), where the seismic ground motion is completely attenuated upon liquefaction (i.e. r_u = 1), while the applied shear stresses are drastically reduced and practically diminish. On the opposite side, of the "thin" layer (Figure 2a), the ground motion and the associated shear stresses remains practically un-altered during the entire shaking period, despite the fact that liquefaction (i.e. r_u = 1) has occurred very early during shaking.

It is speculated that the differences observed in Figure 2 may be traced back to the effect of liquefaction on the natural period of vibration of the soil column. Namely, liquefaction of the "thick" sand layer reduces drastically the shear wave velocity of the sand, as explained in later sections of this paper, and shifts the natural period of the soil column far above the fundamental excitation period, thus triggering the observed seismic isolation effect. On the other hand, the increase of the natural period of the soil column in the case of the "thin" soil layer is marginal, mainly due to the small thickness of that layer compared to the height of the column, and consequently, it may lead to some amplification or de-amplification of the seismic motion, depending on the initial value of the natural soil period relative to the excitation period. It is also interesting to observe that, the sand response in the latter case becomes extremely dilative upon liquefaction, with the r_u values in Figure 2a ranging between r_u = -0.80 and 1.00. It is thus possible that the degradation of the associated shear wave velocity is less than in the former case of the "thick" sand layer, restraining further the increase of the natural soil period and preventing the drastic attenuation of the seismic ground motion amplitude. It is acknowledged that the interaction mechanisms described above are not yet fully understood, as they are interrelated and their factual identification becomes rather involved.

Critical Thickness of Liquefied Layers

The previous findings suggest that effective attenuation of the seismic ground motion requires that the thickness of the liquefiable sand layer exceeds a minimum value, denoted "critical thickness" (H_{cr}) hereafter. The criterion for the estimation of H_{cr} is based on the observation that, in all parametric analyses, predicted seismic ground motions were stabilized at the attenuated state when the thickness of the liquefiable sand layer exceeded H_{cr}. This is explained in Figure 3d, which shows the evolution of the elastic response spectra at the interface clay crust - sand interface as the thickness of the later increased from 1m to 12m. Observe that spectral accelerations over a wide period range converge to their lower bound values for $H_{liq} \geq$ 7m, implying that this is the target critical thickness for the specific set of parametric analyses. The acceleration time-histories for $H_{liq} = H_{cr}$, as well as for the previous and for the next value of H_{liq} are also plotted in Figure 3, in order to demonstrate the transition to the completely attenuated state. It is also interesting to observe here that spectral accelerations increase disproportionally for $H_{liq} \leq$ 2m, verifying our previous conclusion that the liquefaction of relatively "thin" layers is not expected to cause any significant attenuation of the seismic ground motion.

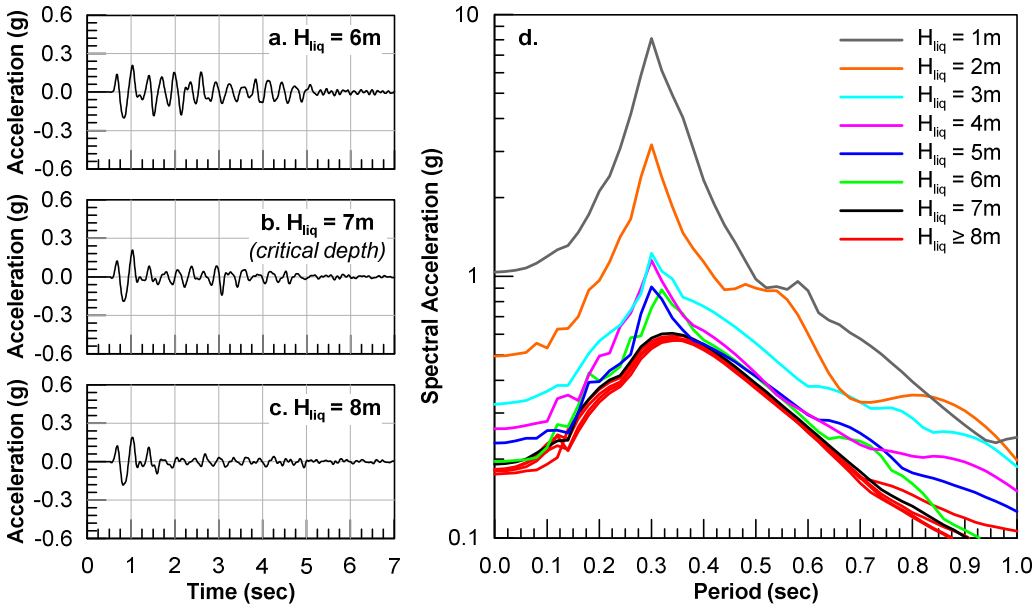

Figure 3. Typical acceleration time-histories at the sand surface for the critical thickness, as well as the previous and the next value of H_{liq} and the corresponding response spectra.

The procedure of Figure 3 was followed for all parametric analyses and the resulting H_{cr} values were subsequently correlated with the basic input parameters, namely the excitation period (T_{exc}), the relative density, the coefficient of permeability, the maximum acceleration of the excitation and the crust thickness. It was thus observed that the relative density and the excitation period have the most systematic and significant effect, as H_{cr} increases steadily for more dense sands and for larger seismic excitation periods. The remaining parameters had a less pronounced effect which was practically eliminated as the associated parameter values increased beyond a relatively low threshold level.

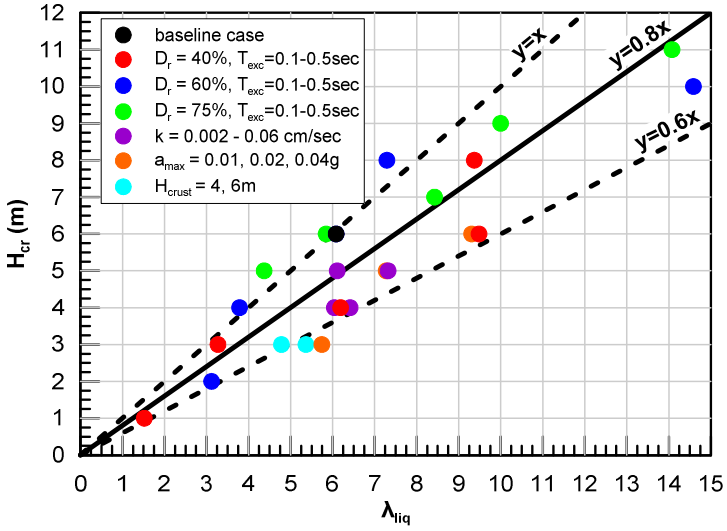

Figure 4. Correlation of H_{cr} to λ_{liq} for the sum of the parametric analyses.

Based on the above remarks, the critical depth is subsequently correlated to the wave length of the liquefied ground, λ_{liq}:

$$\lambda_{liq} = V_{S,liq} \cdot \mathrm{T}_{exc} \tag{1}$$

where $V_{S,liq}$ is the shear wave velocity of the liquefied ground. In this way, the significant effect of the excitation period is directly taken into account, while the effect of relative density is indirectly taken into account through $V_{S,liq}$. This correlation is presented in Figure 4 for the entire set of parametric analyses, using symbols of different color to identify the variation of the different input parameter. Observe that, despite that the critical depth varies widely from H_{cr} = 1m to 11m, its normalized value has a significantly smaller variation from H_{cr}/λ_{liq} = 0.60 to1.00, without any visible bias against some input parameter. Thus, the proposed criterion for the estimation of H_{cr} is based on the mean value of this range and is expressed as:

$$H_{cr} \cong 0.80 \cdot \lambda_{liq} \tag{2}$$

From a different point of view, Eq. (2) can be utilized for the estimation of an upper bound "critical frequency" f_{cr} below which the harmonic excitation components will be filtered out by a liquefiable soil layer with thickness equal to H_{liq}:

$$f_{cr} \cong 0.80 \cdot V_{S,liq} / H_{liq} \tag{3}$$

Shear wave Velocity of Liquefied Ground $V_{S,liq}$

Use of Eqs. (1) and (2) for the estimation of H_{cr} introduces a new soil parameter, namely the shear wave velocity of the liquefied ground $V_{S,liq}$. This parameter is numerically estimated for all parametric numerical analyses, using the "pulse method" explained in Figure 5. More specifically, after the end of the seismic excitation, a single sine pulse with maximum acceleration a_{max} = 0.03g and period T_{exc} = 0.5sec is applied at the base of the soil column. A "quiet" period of 2 - 3sec is left between the end of shaking and the initiation of the pulse, so that the free vibration of the soil column attenuates, while the maximum acceleration and the period of the sine pulse were determined following sensitivity parametric analyses. The average (over the sand thickness) $V_{S,liq}$, is then estimated from the lag Δt in the first arrival time of the pulse at the top and the bottom of the liquefied sand layer (Figure 5), as:

$$V_{S,liq} = H_{liq} / \Delta t \tag{4}$$

The same procedure was also followed before the application of the seismic excitation and led to the estimation of the average initial (prior to excess pore pressure buildup) shear wave velocity of the sand layer, $V_{S,o}$. It was thus found that, for all parametric analyses, the post- to pre-shaking shear wave velocity ratio varied in the more or less constant range $V_{S,liq}/V_{S,o}$ = 0.10 – 0.25 (Figure 5b), without any prominent effect of the various input soil and excitation parameters. These values are in good agreement with previous independent studies (Davis & Berrill 2001; Elgamal et al. 1996; Miwa & Ikeda 2006; Pease & O'Rourke 1997; Zeghal & Elgamal 1994), which are based on inverse analyses of actual seismic recordings in liquefied areas.

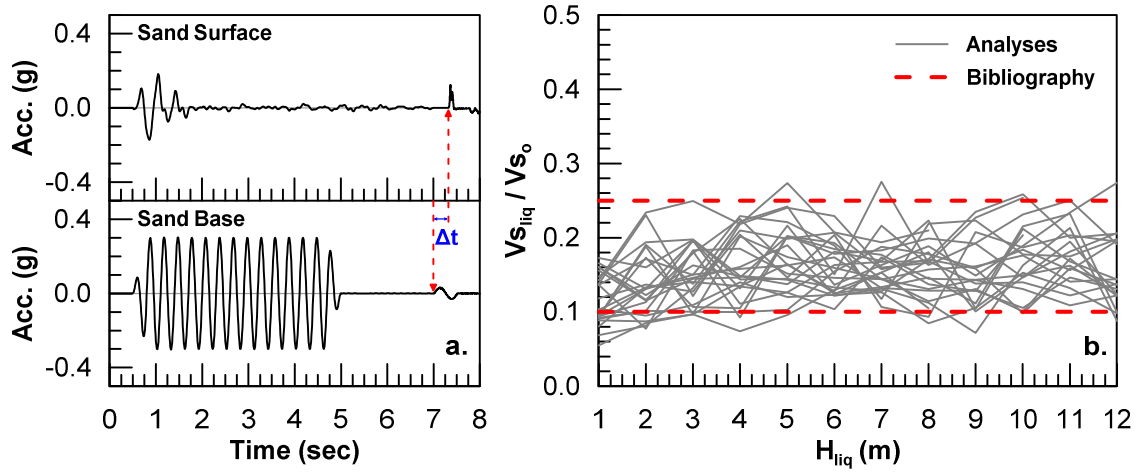

Figure 5. Numerical evaluation of $V_{S,liq}$ and correlation between the $V_{S,liq}/V_{S,o}$ ratio and H_{liq}.

Further reference to the shear wave velocity of the liquefied ground is given in the following chapter, in connection with the simplified estimation of the elastic response spectra of liquefiable sites. It should only be added here that, in view of this seemingly unique correlation between $V_{S,liq}$ and $V_{S,o}$, the critical thickness of the liquefiable sand layer may be alternatively related to the pre-shaking average wave length of the natural ground $\lambda_{o,}$ which is easier to compute ($\lambda_o = V_{S,o} \cdot T_{exc)}$. Namely, for the above range of the $V_{S,liq}/V_{S,o}$ ratio, Eqs. (2) & (3) are re-written as:

$$H_{cr} \cong (0.08 - 0.20)\,\lambda_o \qquad (5), (5a)$$

and

$$f_{cr} \cong (0.08 - 0.20) \cdot V_{S,o} / H_{liq} \qquad (5b)$$

Simplified Estimation of Elastic Response Spectra: the "INTERPOLATION" Method

Background and Methodology Outline

The majority of the reviewed field and experimental case studies show that liquefaction will cause de-amplification of the peak ground surface acceleration, *PGA*. However, we have also spotted evidence for the opposite, in cases when liquefaction occurred after the strong motion part of the seismic excitation (e.g. the liquefaction case study in Wildlife Liquefaction Array, WLA, under Superstition Hills earthquake) or in the presence of relatively thin (e.g. approximately 3m thick) liquefiable soil layers (e.g. Dashti et al. 2010). The relative density of the liquefiable soil seems to be related to the *PGA* (e.g. Dashti et al. 2010; Taiebat et al. 2010), for one at least reason: the resistance to liquefaction increases with relative density and consequently the onset of liquefaction may be delayed beyond the strong motion part of the seismic excitation, leading thus to amplification of the seismic motion. Liquefaction effects on spectral accelerations are different for small and for large structural periods, *T*. In the low period range, the effect is similar to the abovementioned one for *PGA*. For the high period range

(approximately for T > 0.8–1.0 sec), liquefaction of the subsoil generally leads to amplification of spectral accelerations (e.g. Youd & Carter 2005; Dashti et al. 2010; Kramer et al. 2011).

Our literature survey did not reveal any widely used methodologies for the definition of design spectra for liquefied sites. The few available methods are clearly approximate, while they are not generally consistent with the above field and experimental observations. For instance, Miwa & Ikeda (2006) propose to use equivalent linear analyses for the prediction of the seismic motion on the surface of the liquefied ground, using constant values of elastic shear modulus for the liquefied soil layers. The key parameter for this kind of analyses is the shear wave velocity of the liquefied ground $V_{S,liq}$, which was estimated by inverse analyses of actual recordings in liquefied sites and was consequently related to the factor of safety against liquefaction, FS_L, and the initial shear wave velocity without liquefaction, $V_{S,o}$ (Table 1). It is noted that Miwa & Ikeda do not provide any details for the hysteretic damping ratio ξ_{liq}, of the liquefied soil that should be used in their analyses. To fill this gap, one may rely on previous findings of Pease & O'Rourke (1997) suggesting that the hysteretic damping ratio of liquefied sands, obtained from reverse analysis of relevant seismic recordings, is $\xi_{liq} = 20-30\%$.

Table 1. Proposed $V_{S,liq}/V_{S,o}$ ratios by Miwa & Ikeda (2006)

$\mathbf{FS_L}$	0.3 - 0.6	0.6 - 0.9	0.9 - 1.0
$\mathbf{V_{S,liq}/V_{S,o}}$	0.10 - 0.14	0.12 - 0.16	0.14 - 0.19

It is commented that the above methodology is conceptually applicable only in the case of extensive liquefaction (e.g. FS_L < 0.40), when liquefaction occurs early during shaking, i.e. well before the peak of the seismic excitation. In the opposite case, this approach may prove significantly non-conservative, since it totally ignores the possible amplification of the seismic excitation segment preceding the onset of liquefaction. This effect is taken indirectly into account by Kramer et al. (2011 & 2015), who proposed numerically established spectral acceleration correction curves (ratio of liquefied over non-liquefied site response spectra) in terms of FS_L. Nevertheless, the Authors acknowledge that application of the proposed correction curves in practice may be premature due to the large scatter of the associated numerical predictions.

The basic assumption of the "interpolation" method proposed herein is that the response spectrum of the liquefied ground (Sa_{REAL}) can be estimated through linear interpolation between the response spectra obtained from equivalent linear analyses for "non-liquefied" (Sa_{NL}) and for totally "liquefied" ground (Sa_L). Note that Sa_L can be computed according to the logic of Miwa & Ikeda (2006), namely with constant $G_{liq} = \rho V_{S,liq}^2$ and hysteretic damping ratio obtained from common ξ-γ empirical curves for sands. Hence:

$$Sa_{REAL}(T) = Sa_{NL}(T) + \alpha(T) \cdot \left[Sa_{NL}(T) - Sa_L(T) \right] \tag{6}$$

It is important that the interpolation factor α, is not unique for the entire response spectrum, but varies with structural period, T. Furthermore, in absence of liquefaction (i.e. FS_L > 1), it is evident that the response spectrum tends to the spectrum for the "non-liquefied" ground and

consequently $\alpha(T)$ tends to zero. On the other hand, for extensive liquefaction, i.e. when the factor of safety is close to zero, the ground liquefies at the early stages of shaking and the response spectrum becomes equal to the "liquefied" one, so that $\alpha(T)$ tends to unity. Hence, it is concluded that the interpolation factor $\alpha(T)$ is also a function of FS_L while its values are restricted to the range $\alpha(T) = 0 - 1$.

Inverse (back-) Calculation of the Interpolation Factor α(T)

At the present stage of our study, calibration of the interpolation factor was based on: (a) three liquefaction case histories, where acceleration recordings were available both at the soil surface and at the base of the liquefied layer, and (b) results of parametric, fully coupled, non-linear, numerical analyses for a liquefiable site with well-known geotechnical profile.

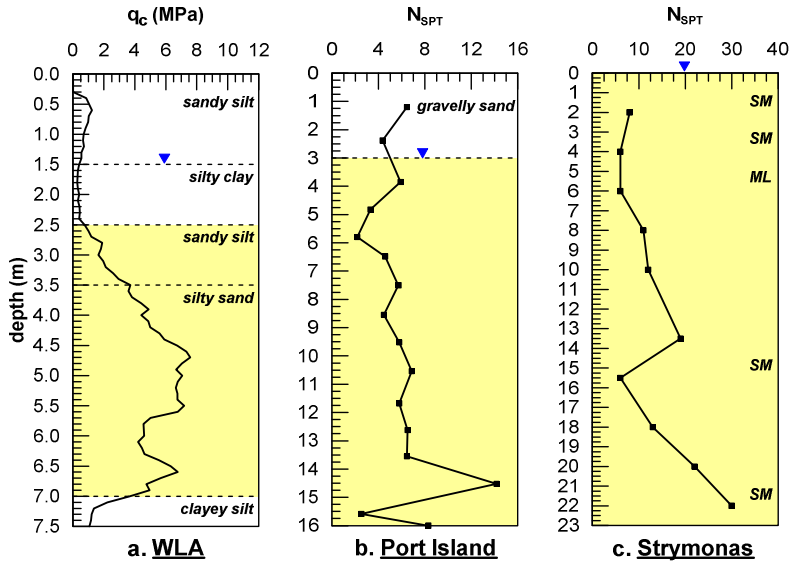

Figure 6. Soil profile and CPT/SPT results for (a) WLA site, (b) Port Island site, and (c) the numerical simulations (at Strymonas river).

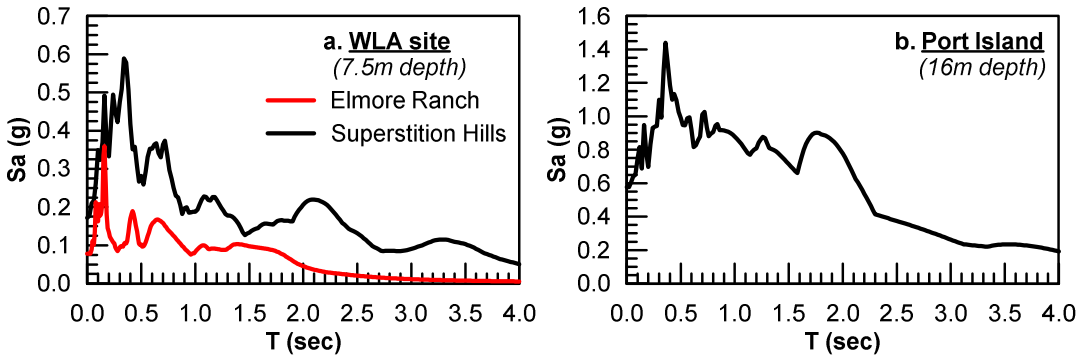

Figure 7. Response spectra at the base of the liquefied layer at (a) WLA (Elmore Ranch and Superstition Hills earthquakes) and (b) Port Island (Kobe earthquake).

The case histories come from the "Wildlife Liquefaction Array" (WLA) in U.S.A. and the "Port Island" array in Japan. The first site consists of 4.5m liquefiable silty sand (2.5 – 7.0m depth), with two accelerometers installed at the soil surface and at 7.5m depth. The respective soil profile, along with the variation of the average tip resistance from 5 CPT tests (Bennett et al. 1984) with depth, is presented in Figure 6a. Two strong motion recordings were obtained in WLA: Elmore Ranch earthquake (1987) of M_w = 6.2 magnitude, which did not cause liquefaction ($FS_L \approx 1.5$) and Superstition Hills earthquake (1987) of M_w = 6.6, which led to liquefaction ($FS_L \approx 0.8$).The Port Island site, consists of loose sand and gravel, which liquefied between 3 – 16m depth during Kobe earthquake (1995) of M_w = 6.9, as $FS_L \approx 0.4$. Acceleration time-histories have been recorded at the ground surface, at 16m depth, as well as at greater depths. The respective soil profile with SPT results (Ishihara et al. 1996) is presented in Figure 6b.

Table 2. Summary of earthquake motions and average FS_L for the numerical simulations.

Motion #	Seismic Scenario A				Seismic Scenario B			
	Seismic Motion	PGA (g)	$FS_{L,av}$	$FS_{L,min}$	Seismic Motion	PGA (g)	$FS_{L,av}$	$FS_{L,min}$
1	*ITALY-BAG*	0.180	0.96	0.87	*NEWZEAL*	0.280	0.88	0.81
2	*ITALY-VLT*	0.136	1.15	1.05	*NORTHR-BLD*	0.251	1.01	0.93
3	*KOBE-AMA*	0.394	1.02	0.94	*NORTHR-CEN*	0.589	0.58	0.53
4	*KOBE-KAK*	0.330	0.73	0.67	*NORTHR-FLE*	0.172	1.05	0.96
5	*KOBE-TDO*	0.383	0.69	0.63	*SFERN-L*	0.150	0.91	0.83
6	*LOMAP-AND*	0.320	0.68	0.62	*SFERN-PEL*	0.211	0.96	0.88
7	*LOMAP-GIL*	0.484	0.57	0.52	*SPITAK*	0.207	0.75	0.69

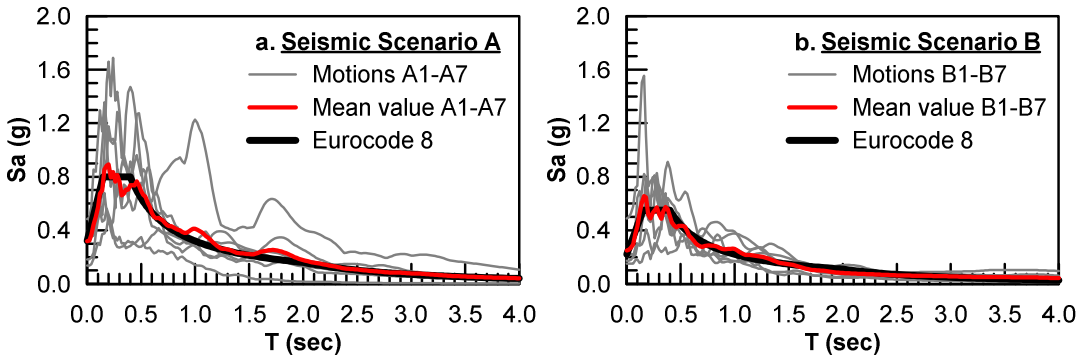

Figure 8. Comparison of the average elastic response spectra at bedrock outcrop for the seismic scenarios A and B with the respective design spectra of EC8.

The numerical analyses simulate the seismic response of an actual soil profile (Figure 6c), located within the riverbed of Strymonas river in Northern Greece, consisting of a 23m thick liquefiable silty sand layer. The seismic response of this site has been simulated with the methodology described in the previous chapter, i.e. with the finite difference code FLAC and the

in-built Critical State soil plasticity model NTUA-Sand. To capture the liquefaction resistance of the in-situ soils, the NTUA-Sand model was properly calibrated against the associated FS_L values, computed from the reported SPT results according to the Youd et al. (2001) empirical method. To examine the effect of shaking magnitude, two different seismic excitation scenarios were considered: the first (scenario A) for T_{ret} = 1000yrs return period, M_w = 7 and PGA = 0.32g at the outcropping bedrock and a second one (scenario B), for T_{ret} = 225yrs, M_w = 6.7 and PGA = 0.22g respectively. For each scenario, a suite of seven earthquake motions with the target magnitude, recorded at bedrock outcrop, is selected and properly scaled so that the average response spectrum is in good agreement with the design spectra of Eurocode 8 for soil type B (Figure 8). These seismic motions, along with the respective average and minimum FS_L values over the liquefiable oil layers are summarized in Table 2. Note that the minimum safety factor values ($FS_{L,min}$) are those of the smoothed FS_L variation, obtained using the "running average" technique and averaging span approximately equal to the critical thickness of this profile, estimated as H_{cr} = 8m. A more detailed explanation about the necessity of this procedure is provided in the description of the "superposition" methodology.

Inverse calculation of the interpolation factors $\alpha(T)$, was based on equivalent linear analyses of each soil profile in Figure 6, performed separately for "non-liquefied" and for "liquefied" ground conditions. For the examined case histories, these analyses were performed using the respective recording at the base of the liquefied layer, shown in Figure 7, whereas the analyses for the Strymonas river site were performed assuming that the input seismic motions of Figure 8 apply at the outcropping bedrock. The equivalent linear analyses for the "liquefied" ground conditions were performed parametrically, for a wide range of liquefied shear wave velocities, in order to find the $V_{S,liq}/V_{S,o}$ ratio which provides the best overall fit of the target elastic response spectrum at long periods (T > 0.8 – 1.0sec).

There are two (2) key parameters that need to be determined, in order to apply the proposed methodology in practice: the $V_{S,liq}/V_{S,o}$ ratio and the variation of coefficient $\alpha(T)$ with period. Starting with the $V_{S,liq}/V_{S,o}$ ratio, the values obtained from the inverse analyses are plotted against the average safety factor ($FS_{L,av}$) in Figure 9a, in comparison with the range proposed by Miwa & Ikeda (2006) for $FS_{L,av} \leq 1$ (Table 1). The observed agreement is fairly good and suggest that the same chart, properly extended for $FS_{L,av}$ > 1.0, may be used for the a-priori selection of $V_{S,liq}/V_{S,o}$ ratio. Typical results from the back-calculation of the interpolation coefficient $\alpha(T)$ are shown in Figure 10, for two numerical simulations of the Strymonas river site. Observe that, in both simulations, the variation of α with T is quite irregular but follows a quite distinct trend. Namely, it exhibits a step-like increase from $\alpha \approx \alpha_{PGA}$ for T < 0.8sec to α = 1 for T > 1sec. A smooth relation that may be used to describe this trend (red line curve in Figure 10) is:

$$\alpha(T) = \left(\frac{1+\alpha_{PGA}}{2}\right) + \left(\frac{1-\alpha_{PGA}}{2}\right)\tanh\left[10\left(T-0.8\right)\right] \tag{7}$$

The lower limit value α_{PGA} in Eq. (7) has been subsequently related in b to the minimum FS_L of the two case studies and all parametric numerical analyses for Strymonas river site. As expected, α_{PGA} degrades smoothly from α_{PGA} =1 at $FS_{L,min} \approx 0$ (severe liquefaction) to $\alpha_{PGA} \approx 0$ at $FS_{L,min}$ > 1.20 – 1.40 (no liquefaction). This variation may be expressed analytically as follows:

$$\alpha_{PGA} = \frac{1}{2}\left\{1+\cos\left[\frac{\pi}{2}\left(\frac{FS_{L,\min}}{\beta}\right)^{1.20}\right]\right\} \quad (8)$$

where $\beta = 0.67 - 0.82$, with a mean value of $\beta = 0.75$.

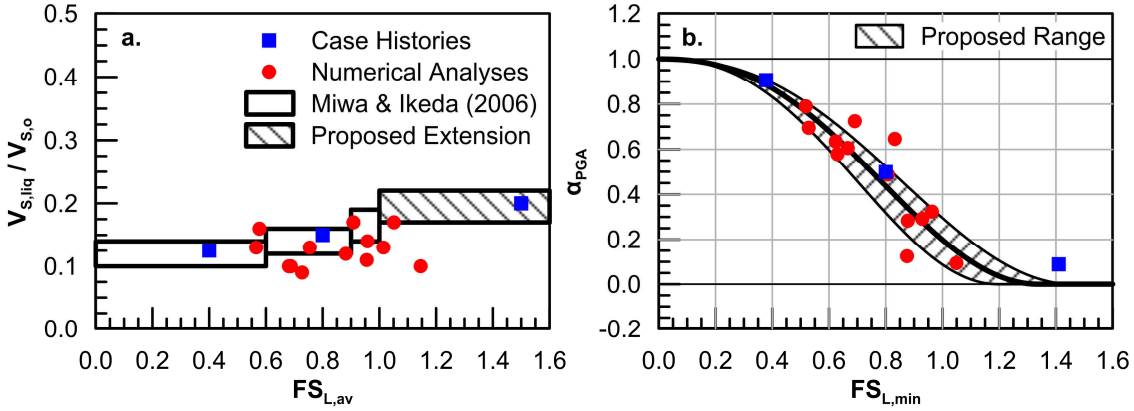

Figure 9. Empirical charts for the computation of $V_{S,liq}/V_{S,o}$ and α_{PGA} in terms of FS_L.

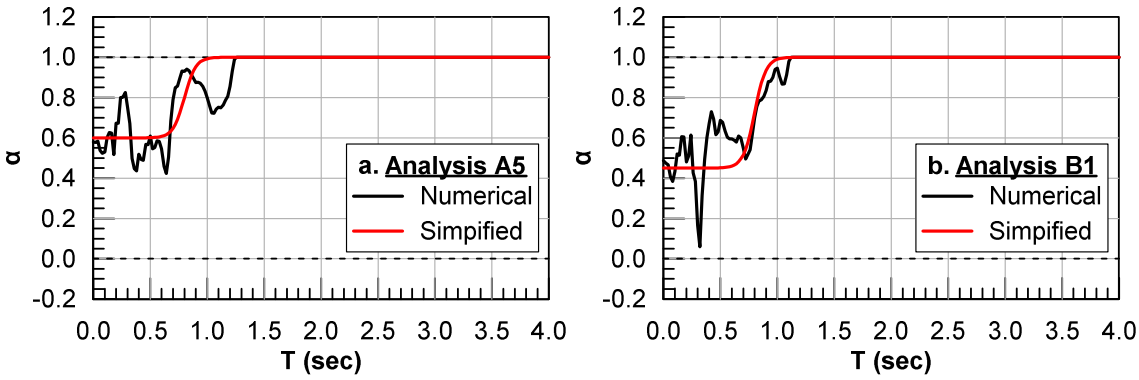

Figure 10. Typical results for the spectral variation of the interpolation coefficient $\alpha(T)$.

Evaluation of Analytical Predictions

To evaluate the accuracy of the proposed methodology, the predicted response spectra (Sa_{PRED}) are compared in Figure 11 with the recorded response spectra at WLA and Port Island liquefaction sites and the numerically simulated ones for seismic scenarios A5 and B1. In all cases, the comparison between the predictions with the proposed methodology and the target response spectra is consistently good, over the entire range of period T. To further appreciate the capabilities of the proposed methodology, predictions using the approach of Miwa & Ikeda (2006) are also plotted in Figure 11. Observe that this early approach provides reliable predictions only in the high period range, and significantly underestimates spectral accelerations in the period range of common structures ($T = 0.3 - 0.6$ec). Exception is the case of Port Island liquefaction site, where liquefaction occurs at the initial stages of shaking ($FS_L \approx 0.4$), and hence, the Miwa & Ikeda (2006) approach provides a reasonable fit of the recorded seismic response.

A more systematic comparison of predicted and target response spectra, in terms of average spectral accelerations over specific ranges of the structural period (i.e. T=0 – 0.15, 0.15 – 0.40, 0.40 – 0.80 & 0.80 – 1.60sec) was performed for all case studies and numerical analyses considered in this paper, with equal success. However, it is not included here due to lack of space.

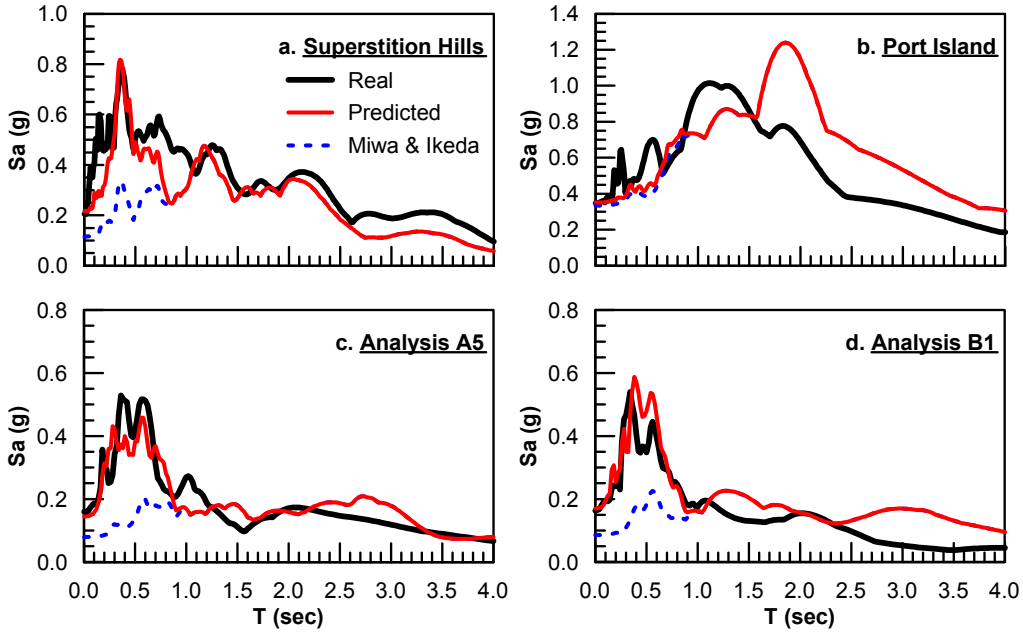

Figure 11. Evaluation of the proposed "interpolation" methodology for (a) WLA during Superstition Hills earthquake, (b) Port Island, (c) analysis A5 and (d) analysis B1.

Simplified Estimation of Elastic Response Spectra: the "SUPERPOSITION" Method

Background and Methodology Outline

The basic assumption of the "superposition" methodology is that the seismic ground response is affected by liquefaction after the excess pore pressure ratio in adequately thick subsoil layers exceeds a certain level, approximately equal to $r_u = 0.40 - 0.60$. The reason for that is realized if one considers that the shear wave velocity of soils is proportional to the fourth root of $1\text{-}r_u$ and consequently the change in the natural vibration period of the liquefied soil is marginal (i.e less than 15 – 25%) for lower r_u values. Field evidence for this assumption is provided in the work of Youd & Carter (2005), who compared the recorded response spectra at the surface of WLA during Superstition Hills earthquake for the entire duration of the seismic excitation and for the first 15sec (Figure 12c). Note that the effects of liquefaction on the seismic motion of the ground surface became apparent after 18.5sec of shaking (Figure 12a), while at the end of the first 15sec the recorded excess pore pressure ratio was less than $r_u \approx 0.20$ (Figure 12b). It was thus observed that the response spectrum for $T < 0.8$sec is controlled by the first part of the seismic excitation, as the two spectra match perfectly over this period range.

Taking further into account that the response spectra at the long period range (i.e. T > 0.8 – 1.0sec) reflect the response of the liquefied ground, as discussed in the literature review and the evaluation of the "interpolation" method of the previous chapter, it is proposed to:

(a) Separate the input seismic motion in 2 parts, the first for $t \leq t_{L,gr}$ and the second for $t > t_{L,gr}$, where $t_{L,gr}$ corresponds to the trigger time of liquefaction effects on the seismic motion of the ground surface.
(b) Perform separate equivalent linear analyses for each part of the input seismic motion, using the non-liquefied soil properties for the first part and the liquefied soil properties for the second part (same as in the Miwa & Ikeda, 2006 methodology).
(c) Define the elastic response spectrum as the envelope of the response spectra computed for the first and the second part of the seismic motion.

The major challenge in applying the above (otherwise simple) methodology is to estimate correctly the time $t_{L,gr}$ at the onset of liquefaction effects on the seismic ground motion. This issue is addressed in the following.

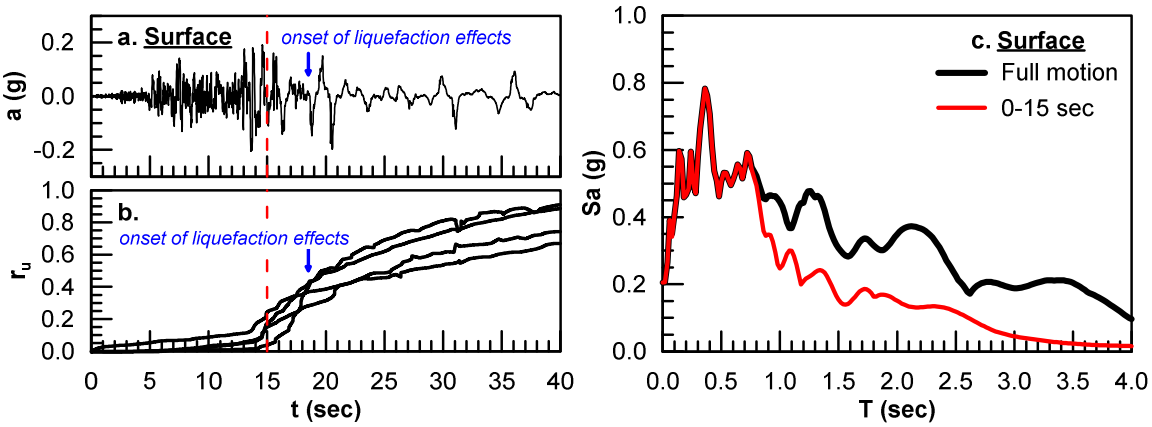

Figure 12. Onset of liquefaction and response spectra at the surface of WLA during Superstition Hills earthquake for the entire recorded seismic motion and for the first 15sec.

Estimation of Liquefaction Onset Time $t_{L,gr}$

For a single sand layer and harmonic seismic shaking with period equal to T_{exc}, the liquefaction onset time is $t_L = N_L \cdot T_{exc}$, where N_L denotes the number of loading cycles required to cause liquefaction under constant applied shear stress ratio *CSR*. On the other hand, there is ample experimental evidence (e.g. Tokimatsu & Yoshimi 1983; Liu et al. 2001; Idriss & Boulanger 2008; Cetin & Bilge 2012; Kishida & Tsai 2014) that the cyclic resistance stress ratio *CRR* may be related with the applied number of cycles N_{EQ} with a power law, i.e.:

$$CRR = a \cdot N_{EQ}^{-b} \tag{9}$$

where coefficient a and exponent b depend on soil type and loading conditions. Thus, the factor of safety against liquefaction is finally written as:

$$FS_L = \frac{CRR}{CSR} = \left(\frac{N_L}{N_{EQ}} \right)^b \tag{10}$$

and consequently the liquefaction onset time t_L may be computed in terms of FS_L, as:

$$t_L = T_{exc} \cdot N_{EQ} \cdot FS_L^{1/b} \tag{11}$$

For practical applications, when the empirical methodology of Youd et al. (2001) is used to compute FS_L, exponent b in Eqs. (9) & (11) may be indirectly computed from the recommended expression for the magnitude scaling factor *MSF*:

$$MSF = \frac{CRR_{M_w}}{CRR_{M_w=7.5}} = \frac{10^{2.24}}{M_w^{2.56}} \tag{12}$$

and the Seed & Idriss (1982) correlation of earthquake magnitude M_w to equivalent harmonic loading cycles N_{EQ} of Table 3. Namely, when the resulting $MSF - N_{EQ}$ graph is plotted in a double logarithmic scale, it may be readily fitted by a linear relationship to give a negative slope corresponding to $b = 0.55$.

Table 3. Equivalent number of cycles due to earthquake loading (Seed & Idriss 1982)

M_w	5.25	6	6.75	7.5	8.5
N_{EQ}	2- 3	5 - 6	10	15	26

Application of Eq. (11) to actual seismic excitations, with irregular acceleration time history, requires definition of an "equivalent" harmonic motion with N_{EQ} loading cycles, excitation period, T_{exc}, and constant acceleration amplitude, equal to the effective acceleration value, a_{eff}. In the present study, this transformation is based on the following algebraic equation:

$$a_{eff} T_{exc}^2 N_{EQ} = \pi^2 \int_{t=0}^{N \cdot T} |v(t)| dt \tag{13}$$

which yields to:

$$N_{EQ} = \frac{\pi^2 \int_{t=0}^{N \cdot T} |v(t)| dt}{a_{eff} T_{exc}^2} \tag{14}$$

where $v(t)$ denotes the time-history of the seismic velocity. Note that Eqs. (13) & (14) are strictly accurate for harmonic excitations, but also provide reasonable estimations of N_{EQ} for the analytical computation of liquefaction related effects under irregular seismic loading (e.g. Karamitros et al., 2013). From a sensitivity analysis performed during the present study, it was found that consistent N_{EQ} estimations are obtained when the predominant excitation period T_{exc} in Eq. (14) is taken as the mean period for $Sa \geq 2.5 \cdot PGA$, while the effective acceleration is calculated according to Tokimatsu & Yoshimi (1983), as:

$$a_{eff} = \left[(M_w - 1)/10 \right] a_{\max} \tag{15}$$

The previous derivation applies to single sand layers and may be used to estimate the variation with depth of the associated liquefaction onset time $t_L(z)$ within a given liquefiable soil profile and a given acceleration time history for the seismic excitation. The liquefaction onset time at the ground surface $t_{L,gr}$ is of course related to, but differs from the specific $t_L(z)$ values as it reflects the response of the entire soil column and not that of any particular liquefiable soil layer. Based on our previous findings regarding the isolating capacity of liquefiable soil layers, it was next attempted to correlate $t_{L,gr}$ to the $min(t_L)$ of a given soil profile while taking also into account the thickness of the corresponding sand layer.

The data, which were used for that purpose came from about 100 parametric numerical analyses, performed with the methodology and the soil profiles used to study the seismic isolation effects (i.e. Figure 1) and five of the actual seismic excitations of Table 2 (A5, A6, B1, B4 & B6) scaled to two different peak acceleration levels, approximately equal to 0.15g and 0.30g. Taking into account that the soil column was discretized into 0.50m thick zones, the computed t_L variation with depth was smoothed using the "running average" technique, so that the $min(t_L)$ corresponds to layers with a substantially larger thickness. From a trial-and-error parametric analysis, for various running average intervals, it was thus found that a best fit correlation is obtained for 3m intervals (equivalent to 3m thick soil liquefiable soil layers). It is noteworthy that, although independently computed, this thickness falls within the range of critical thickness H_{cr} values of the analyzed profiles computed from Eq. (5)

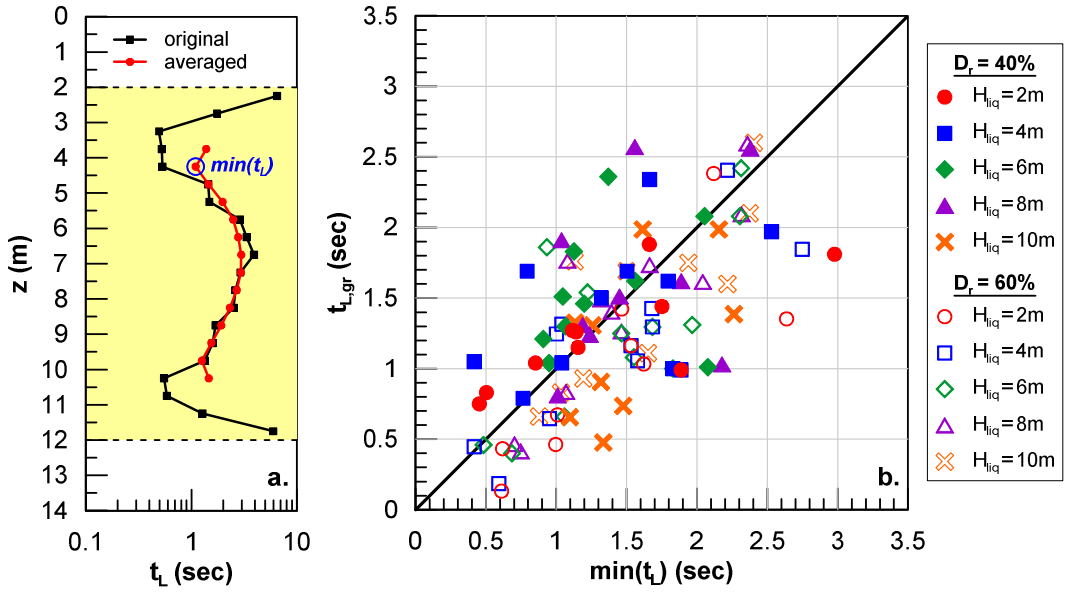

Figure 13. (a) Typical t_L profiles from parametric numerical analyses, before and after smoothing with 3m "running average" interval, (b) one-to-one comparison between $t_{L,gr}$ and $min(t_L)$

The best fit $t_{L,gr}$ vs $min(t_L)$ comparison is shown in Figure 13, with symbols of different color and shape used to differentiate the relative density (D_r = 40 & 60%) and the thickness (H_{liq} = 2, 4, 6, 8 & 10m) of the liquefiable sand layer respectively. Note that none of the above parameters seems to have a systematic effect on $t_{L,gr}$ while there is also no bias with regard to the magnitude of $min(t_L)$. Hence, on average, it may be assumed that:

$$t_{L,gr} = \min(t_L) \tag{16}$$

For conservative elastic response spectra predictions, $t_{L,gr}$ may be somewhat increased in order to cover a larger percentage of the comparison data points.

Evaluation of Analytical Predictions

The proposed "superposition" methodology has been evaluated for the same 17 cases as in the interpolation methodology, i.e. the three liquefaction case histories, and the fourteen numerical analyses at Strymonas river site. The values of the calculated minimum FS_L, which are necessary for the estimation of $t_{L,gr}$, have been presented in Table 2, the number of cycles are estimated from the input acceleration (recorded at the base for the case histories or applied as outcropping bedrock motion in the numerical simulations), whereas the $V_{S,liq}/V_{S,o}$ ratio for the totally liquefied analysis is selected from Figure 9a. In summary, the basic steps of the superposition methodology are shown in Figure 14, for the case of numerical analysis B1.

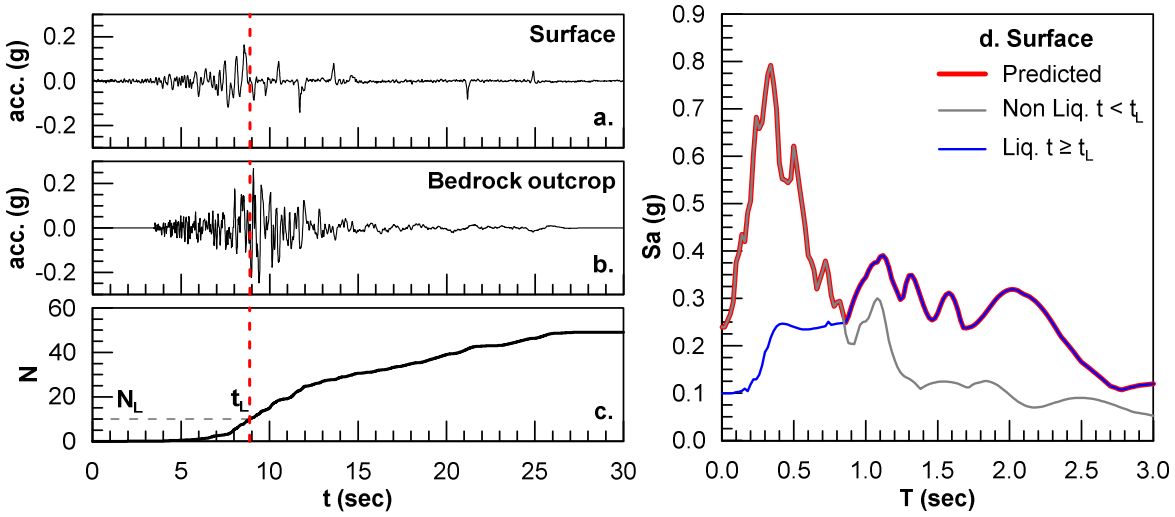

Figure 14. Prediction steps for case B1: Acceleration time-histories (a) at the surface and (b) at the outcropping bedrock, (c) estimation of number of uniform cycles to liquefaction and (d) prediction of elastic response spectra.

The accuracy of the proposed "superposition" methodology is evaluated in Figure 15. In particular, the predicted response spectra are compared with the recorded ones at WLA and Port Island sites and the numerical predictions for seismic scenarios A5 and B1. A good agreement is observed in all cases, not only on peak ground acceleration values but also at the spectral acceleration values for the entire range of periods. As in Figure 11, predictions with the Miwa & Ikeda (2006) approach are also plotted in Figure 15 in order to appreciate the progress achieved. As in the case of the "interpolation" method, presented in the previous chapter, predicted and target response spectra were also compared in terms of average spectral accelerations over specific ranges of the structural period. Those comparisons, not shown here due to space limitations, are also satisfactory for the entire range of examined structural periods.

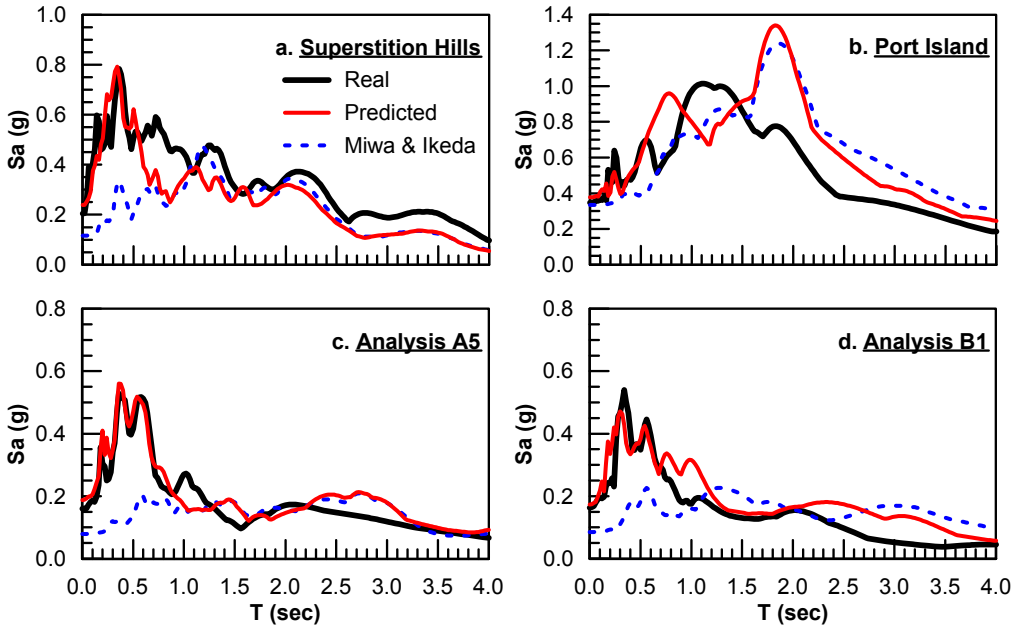

Figure 15. Evaluation of the proposed "superposition" methodology for (a) WLA during Superstition Hills earthquake, (b) Port Island, (c) analysis A5 and (d) analysis B1.

Concluding Remarks

In conclusion, attention is drawn to the following main findings from the presented study:

a) A liquefiable soil layer may amplify or de-amplify the seismic ground motion, depending on two main factors: the onset of liquefaction relative (before or after) to the strong motion part of the seismic excitation, grossly related to the factor of safety against liquefaction FS_L, and the capacity of the layer to attenuate the seismic excitation (i.e. to act as natural seismic isolation).

b) The shear wave velocity of liquefied soil layers is not zero, but attains a residual value $V_{S,liq}$ = (0.10–0.25)$V_{S,o}$, with the $V_{S,liq}/V_{S,o}$ ratio probably increasing with FS_L (Miwa & Ikeda, 2006). This residual value corresponds to excess pore pressure ratio $r_{u,liq}$ = 0.996–0.9999.

c) A liquefied soil layer may effectively attenuate harmonic excitation components with wave length λ_{liq} approximately equal to or less than its thickness H_{liq}. The corresponding wave length for initial (i.e. prior to liquefaction) soil conditions is equal to or less than (5–12.5)H_{liq}, depending on the exact value of the $V_{S,liq}/V_{S,o}$ ratio.

d) For liquefiable sites, the free field elastic response spectra may be approximately predicted with simple (e.g. SHAKE-type) analyses based on "interpolation" between the respective spectra for initial and for completely liquefied soil conditions, or by "superposition" of the elastic response spectra for the pre- and the post-liquefaction part of the seismic excitation. Comparison with data from field case studies and parametric numerical analyses show that the above methods may capture equally well both the pre- and the post-liquefaction components of the seismic ground response.

e) Both simple methods proposed herein rely heavily on computed factors of safety against liquefaction FS_L within the liquefiable site. Trial-and-error application of various

representative FS_L values led to the conclusion that the site response is mostly affected by the minimum FS_L value, averaged over a soil thickness approximately equal to the predominant wave length upon liquefaction λ_{liq}.

It should be noted that the previous findings have been evaluated against data from the few available case histories and a relatively limited number of parametric numerical simulations for an actual soil profile. Work is currently in progress in order to improve our insight to the aforementioned mechanisms of natural seismic isolation and also evaluate the overall benefits in the design of structures from using shallow foundations on liquefiable sites. It is thus possible that the proposed simple analytical relationships and prediction methods are refined in the future, even though minor (if any) changes should be anticipated in the general findings with regard to the mechanisms which control the response of liquefiable sites.

Acknowledgments

This research has been co-financed by the European Union (European Social Fund – ESF) and Greek national funds through the Operational Program "Education and Lifelong Learning" of the National Strategic Reference Framework (NSRF)-Research Funding Program: THALES. Investing in knowledge society through the European Social Fund.

References

Andrianopoulos, K. I., Papadimitriou, A. G., and Bouckovalas, G. D. (2010). "Bounding surface plasticity model for the seismic liquefaction analysis of geostructures." *Soil Dynamics and Earthquake Engineering*, **30**(10), pp. 895–911.

Arulmoli, K., Muraleetharan, K. K., Hossain, M. M., and Fruth, L. S. (1992). "*VELACS: verification of liquefaction analyses by centrifuge studies; Laboratory Testing Program* – Soil Data Report." Research Report, The Earth. Technology Corporation.

Bennett, M. J., McLaughlin, P. V, Sarmiento, J., and Youd, T. L. (1984). "*Geotechnical investigation of liquefaction sites, Imperial Valley, Calif.*" U.S. Geological Survey Open File Report, 84-252.

Cascone, E., and Bouckovalas, G. D. (1998). "Seismic bearing capacity of footings on saturated sand with a clay cap." *Procedings of the 11th European Conference on Earthquake Engineering*.

Cetin, K. O., and Bilge, H. T. (2012). "Performance-Based Assessment of Magnitude (Duration) Scaling Factors." *Journal of Geotechnical and Geoenvironmental Engineering*, **138**(3), 324–334.

Dashti, S., Bray, J. D., Pestana, J. M., Riemer, M., and Wilson, D. (2010). "Mechanisms of Seismically Induced Settlement of Buildings with Shallow Foundations on Liquefiable Soil." *Journal of Geotechnical and Geoenvironmental Engineering*, American Society of Civil Engineers, **136**(1), 151–164.

Davis, R. O., and Berrill, J. B. (2001). "Liquefaction at the Imperial Valley Wildlife Site." *Bulletin of the New Zealand Society for Earthquake Engineering*, **34**(2), 91–106.

Dimitriadi, V. (2014). "Performance Based Design and Soil Improvement Methods of Shallow Foundations on Liquefiable Soils." PhD Thesis, Dept of Civil Engineering, NTUA, Athens.

Elgamal, A.-W., Zeghal, M., and Parra, E. (1996). "Liquefaction of reclaimed island in Kobe, Japan." *Journal of Geotechnical Engineering*, **122**(1), 39–49.

Idriss, M. I., and Boulanger, R. W. (2008). *Soil Liquefaction During Earthquakes*. Earthquake Engineering Research Institute, Oakland, California, USA.

Ishihara, K., Yasuda, S., and Nagase, H. (1996). “Soil characteristics and ground damage.” *Soils and Foundations*, Japanese Soc of Soil Mechanics & Foundation Engineering, 109–118.

Itasca. (2011). “FLAC version 7.0.” *Itasca Consulting Group Inc.*

Iwasaki, Y., and Tai, M. (1996). “Strong motion records at Kobe Port Island.” *Soils and Foundations*.

Karamitros, D., Bouckovalas, G., and Chaloulos, Y. (2012). “Insight into the Seismic Liquefaction Performance of Shallow Foundations.” *Journal of Geotechnical and Geoenvironmental Engineering*, American Society of Civil Engineers, **139**(4), 599–607.

Karamitros, D. K. (2010). “*Development of a Numerical Algorithm for The Dynamic Elastoplastic Analysis of Geotechnical Structures in Two and Three Dimensions*.” PhD Thesis, Dept of Civil Engineering, NTUA, Athens.

Karamitros, D. K., Bouckovalas, G. D., and Chaloulos, Y. K. (2013). “Seismic settlements of shallow foundations on liquefiable soil with a clay crust.” *Soil Dynamics and Earthquake Engineering*, **46**(0), 64–76.

Kawasumi, H. (1968). *General Report on the Niigata Earthquake of 1964*.

Kishida, T., and Tsai, C. C. (2014). “Seismic Demand of the Liquefaction Potential with Equivalent Number of Cycles for Probabilistic Seismic Hazard Analysis.” *Journal of Geotechnical and Geoenvironmental Engineering*, **140**(3), 04013023.

Kramer, S. L., Astaneh Asl, B., Ozener, P., and Sideras, S. S. (2015). “Effects of Liquefaction on Ground Surface Motions.” *Perspectives on Earthquake Geotechnical Engineering - In Honour of Prof. Kenji Ishihara*, Geotechnical, Geological and Earthquake Engineering, Springer International Publishing, 285–309.

Kramer, S. L., Hartvigsen, A. J., Sideras, S. S., and Ozener, P. T. (2011). “Site response modeling in liquefiable soil deposits.” *4th IASPEI / IAEE International Symposium: Effects of Surface Geology on Strong Ground Motion*.

Liu, A. H., Stewart, J. P., Abrahamson, N. A., and Moriwaki, Y. (2001). “Equivalent Number of Uniform Stress Cycles for Soil Liquefaction Analysis.” *Journal of Geotechnical and Geoenvironmental Engineering*, **127**(12), 1017–1026.

Liu, L., and Dobry, R. (1997). “Seismic response of shallow foundation on liquefiable sand.” *Journal of Geotechnical and Geoenvironmental Engineering*, ASCE, **123**(6), pp. 557–566.

Miwa, S., and Ikeda, T. (2006). “Shear modulus and strain of liquefied ground and their application to evaluation of the response of foundation structures.” *Structural Engineering/Earthquake Engineering*, **23**(1), 167s–179s.

Naesgaard, E., Byrne, P. M., and Ven Huizen, G. (1998). “Behaviour of light structures founded on soil ‘crust’ over liquefied ground.” *Geotechnical Special Publication*, **75**, 422–433.

Pease, J. W., and O’Rourke, T. D. (1997). “Seismic response of liquefaction sites.” *Journal of Geotechnical Engineering*, **123**(1), 37–45.

Ramberg, W., and Osgood, W. R. (1943). *Description of stress-strain curve by three parameters*. Technical note 902, National Advisory Committee for Aeronautics.

Seed, H. B., and Idriss, I. M. (1982). “Ground motions and soil liquefaction during earthquakes.” *Ground Motions and Soil Liquefaction during Earthquakes*.

Taiebat, M., Jeremić, B., Dafalias, Y. F., Kaynia, A. M., and Cheng, Z. (2010). “Propagation of seismic waves through liquefied soils.” *Soil Dynamics and Earthquake Engineering*, **30**(4), 236–257.

Tokimatsu, K., and Yoshimi, Y. (1983). Empirical correlation of soil liquefaction based on SPT N-value and fines content. *Soils and Foundations*, 56–74.

Vucetic, M., and Dobry, R. (1991). “Effect of soil plasticity on cyclic response.” *Journal of geotechnical engineering*.

Youd, T., Idriss, I., Andrus, R., Arango, I., et al. (2001). “Liquefaction Resistance of Soils: Summary Report from the 1996 NCEER and 1998 NCEER/NSF Workshops on Evaluation of Liquefaction Resistance of Soils.” *Journal of Geotechnical and Geoenvironmental Engineering*, American Society of Civil Engineers, **127**(10), 817–833.

Youd, T. L., and Carter, B. L. (2005). “Influence of Soil Softening and Liquefaction on Spectral Acceleration.” *Journal of Geotechnical and Geoenvironmental Engineering*, **131**(7), 811–825.

Zeghal, M., and Elgamal, A. W. (1994). “Analysis of site liquefaction using earthquake records.” *Journal of Geotechnical Engineering - ASCE*, **120**(6), 996–1017.